Update on electron-cloud power deposition for the LHC arc dipoles*

Miguel A. Furman†
Center for Beam Physics
Lawrence Berkeley National Laboratory, Bldg. 71R0259
1 Cyclotron Rd.
Berkeley, CA 94720-8211

Vernon H. Chaplin‡
500 College Ave.
Swarthmore College
Swarthmore, PA 19081

(Dated: **DRAFT:** October 28, 2005)

We revisit the estimation of the power deposited by the electron cloud (EC) in the arc dipoles of the LHC by means of simulations. We adopt a set of electron-related input parameters closely resembling those used in recent simulations at CERN [1]. We explore values for the bunch population N_b in the range $0.4 \times 10^{11} \leq N_b \leq 1.6 \times 10^{11}$, peak secondary electron yield (SEY) $\delta_{\max}$ in the range $1.0 \leq \delta_{\max} \leq 2.0$, and bunch spacing t_b either 25 or 75 ns. For $t_b = 25$ ns we find that, for the cooling limit of the cryogenic system (~ 2 W/m) not to be exceeded, $\delta_{\max}$ must not exceed 1.3, and probably needs to be lower than this. For $t_b = 75$ ns our estimated EC power deposition is comfortably below the cooling limit even for $N_b = 1.6 \times 10^{11}$ and $\delta_{\max} = 2$. We also find that the rediffused component of the secondary electron emission spectrum plays a significant role: if we artificially suppress this component while keeping $\delta_{\max}$ fixed, the estimated EC deposition is roughly cut in half, and in this case we find good agreement with the results in Ref. 1. We provide a fairly detailed explanation of the mechanism responsible for such a relatively large effect. We also provide results testing the sensitivity of our results to certain numerical simulation parameters, and to physical parameters such as the photoelectric yield, bunch train length, etc.

I. INTRODUCTION.

The primary concern raised by the electron-cloud effect (ECE) for the LHC is the power deposited on the walls of the beam screen by the electrons rattling around the chamber under the action of the beam. The LHC will be the first proton storage ring ever built in which the circular trajectory of the beam will lead to significant synchrotron radiation as a by-product of the particle motion. At top beam energy the emitted radiation will generate a substantial number of photoelectrons upon striking the chamber. The main uncertainty in the determination of the EC power deposition, however, arises not from the photoelectrons but rather from the compounding effect of secondary electron emission which, when combined with the time structure of the beam, leads to strong time fluctuations in the EC distribution and power deposition, and to a substantial average EC density [2, 3].

Since the cryogenic system required for the superconducting magnets was designed before the discovery of the ECE, the specification of the cooling capacity of the system did not take into account the EC power deposition. As a result, since 1998, significant experimental and theoretical efforts have been devoted at CERN and elsewhere to better estimate the power deposition and to suggest mitigation mechanisms if necessary [4–7]. An early estimate [8], based on a simple physical model, led to 0.2 W/m. Soon thereafter, simulations yielded higher estimates, and showed a rather strong sensitivity to certain parameters, particularly those pertaining to the SEY and the secondary electron spectrum [2, 9–12]. Since many of these parameters are not very well known for the actual materials for the LHC vacuum chamber, this sensitivity makes a firm estimate of the power deposition challenging.

In this article we revisit our previous estimates of the EC power deposition in an arc dipole of the LHC [2, 10, 11]. We use here a set of parameters that is close to, but not identical with, a set used in Ref. 1. Some of these parameters are taken from measurements at CERN [13]. In addition to updating our estimates for the EC power deposition, we confirm and explain in detail the strong effect of the rediffused electrons on the average EC density and power deposition [12]. When we neglect the rediffused electrons while keeping $\delta_{\max}$ fixed, we find good agreement with Ref. 1. We briefly discuss remaining uncertainties, and the implications of our results for the conditioning process during LHC commissioning.

*Work supported by the US DOE under contract DE-AC02-05CH11231 and by the US-LHC Accelerator Research Project (LARP).
†Electronic address: mafurman@lbl.gov; URL: http://mafurman.lbl.gov
‡Electronic address: vchapli1@swarthmore.edu

II. SIMULATION DETAILS.

A. Beam and chamber.

Specifically, we simulate the EC build-up when a bunch train is injected into an empty chamber in an arc dipole magnet of length $L = 14.2$ m and magnetic field $B = 8.39$ T. We let the bunch intensity N_b range in $(0.4 - 1.6) \times 10^{11}$. The bunch spacing t_b is either 25 ns or 75 ns, corresponding to 10 or 30 RF buckets, respectively. For $t_b = 25(75)$ ns the bunch train consists of 72(24) bunches, followed by a gap. The full train consists of 810 buckets, or ~ 2 μs of beam time.[1]

B. Electron sources.

In this note we consider only the two most important sources of electrons within the LHC arc chamber, namely photoemission from the synchrotron radiation striking the walls of the chamber, and secondary electron emission.

At top energy ($E = 7$ TeV, corresponding to a relativistic factor $\gamma_b = 7.46 \times 10^3$), the beam will emit synchrotron radiation with a critical energy $E_{\rm crit} = 44.1$ eV at the rate of $n'_\gamma = 1.27 \times 10^{-2}$ photons per proton per meter of trajectory in the bending magnets of the arcs (we only include in n'_γ those photons whose energy is above 4 eV, ie., the work function of the chamber surface). At nominal intensity, $N_b = 1.1 \times 10^{11}$ protons per bunch, this implies 1.39×10^9 photons per bunch per meter. The effective quantum efficiency per penetrated photon, or photoelectron yield $Y_{\rm eff}$, can be estimated from the photon spectrum, average angle of incidence, and surface properties of the wall. Our simulations take as input the number of photoelectrons generated per proton per unit length of beam traversal, $n'_{e(\gamma)} = Y_{\rm eff}\, n'_\gamma$, rather than n'_γ and $Y_{\rm eff}$ separately, hence we only list $n'_{e(\gamma)}$ in Tables I and II.

We assume the photoelectrons to be emitted from the walls with a spectrum

$$\frac{dN}{dEd\Omega} \propto e^{-(E-E_\gamma)^2/2\sigma_{E\gamma}^2} \times \cos^{\alpha_\gamma}\theta \qquad (1)$$

where E is the kinetic energy of the emitted photoelectron, θ is the emission angle relative to the normal to the surface at the emission point, and the phenomenological parameters E_γ, $\sigma_{E\gamma}$ and α_γ have the values 5 eV, 5 eV, and 2, respectively. The overwhelming number of synchrotron photons are radiated in a fan of rms opening angle $\sim \gamma_b^{-1} = 134$ μrad, and strike the outboard side of the beam screen some ~ 10 m downstream of the radiation point, leading to an illuminated strip of rms height $\sigma_\gamma = 1.4$ mm. We assume that the effective photon reflectivity is $R_\gamma = 0.2$ which means that 80% of the photoelectrons are generated at the illuminated region of the wall with a distribution $dN/dy \propto \exp(-y^2/2\sigma_\gamma^2)$ where y is the vertical direction along the wall relative to the midplane. The remaining 20% of the photoelectrons are generated uniformly around the cross-section of the beam screen.

A conditioning process leads to a gradual decrease of the peak value $\delta_{\rm max}$ of the secondary emission yield (SEY) function $\delta(E_0)$ as the surface is bombarded with electrons [14, 15]. Since we do not know the actual value of $\delta_{\rm max}$ at the start of commissioning, nor how fast it will decrease during operation, we consider here the range $1 \le \delta_{\rm max} \le 2$, which will almost certainly encompass the values of practical interest. Experience has shown that this conditioning process also causes a downshift of the energy $E_{\rm max}$ at which the true secondary component of $\delta(E_0)$ reaches a maximum, and a decrease of the effective photoelectron yield $Y_{\rm eff}$. For simplicity we assume, following Ref. 1, that these shifts are correlated so that $n'_{e(\gamma)}$ and $E_{\rm max}$ interpolate linearly with $\delta_{\rm max}$ between their values at $\delta_{\rm max} = 1$ and $\delta_{\rm max} = 2$. The specific values we use for our simulations are listed in Table II.

The secondary emission model embodied in the code POSINST [2, 16] is based on a probabilistic simulation of the emission process that is described by phenomenological formulas fitted to experimental data. The model and all its parameters are described in detail in Refs. 17–18. Closely related to $\delta(E_0)$ is the emitted-energy spectrum of the secondary electrons, $d\delta/dE$, where E is the emitted electron energy. The spectrum exhibits three fairly distinct main components: elastically reflected electrons (δ_e), rediffused (δ_r), and true secondaries (δ_{ts}), so that $\delta = \delta_e + \delta_r + \delta_{ts}$. The three components depend on incident electron energy and angle, and are qualitatively different from each other. Depending upon various features of the beam and storage ring considered, the three components can contribute differently to different aspects of the ECE. For the purposes of this note we adopt the SEY model corresponding to the copper data in Refs. 17–18, except that here we scale all three components of δ by a common factor so that so that $\delta_{\rm max}$ has the value(s) stated in each simulation case instead of the original 2.05. We define the absolute and relative backscattered components, respectively, as

$$R_e(E_0) = \delta_e(E_0) + \delta_r(E_0)\,, \qquad (2a)$$

$$\tilde{R}_e(E_0) = \frac{R_e(E_0)}{\delta(E_0)} \qquad (2b)$$

and are shown in Fig. 1. Our SEY model has $\tilde{R}_e = 0.1$ at $E_0 = E_{\rm max}$ at normal incidence. According to the above explanation, $R_e(E_0)$ scales proportionally to $\delta_{\rm max}$ while $\tilde{R}_e(E_0)$ remains invariant. In Sec. V we address the validity and possible consequences of this assumption.

[1] Owing to a misunderstanding we chose a train length of 810 buckets, while the actual specification is 800 buckets. The extra 10 buckets in the gap have a negligible effect on our results, however.

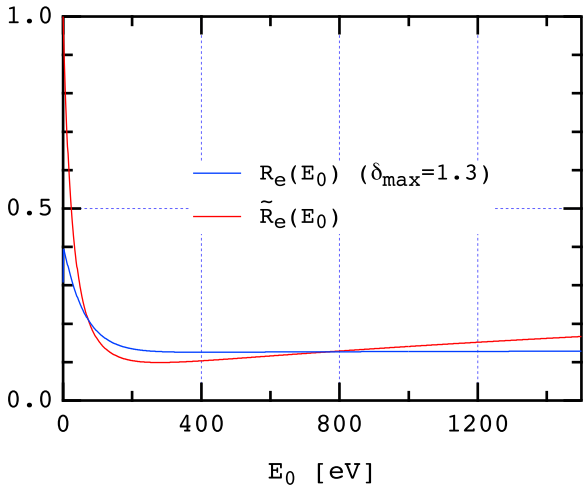

FIG. 1: The absolute ($R_e(E_0)$ and relative ($\tilde{R}_e(E_0)$ backscattered components at normal incidence for our model, Eqs. 2. The absolute component is plotted for $\delta_{\max} = 1.3$. The relative component is independent of $\delta_{\max}$, by construction.

C. Simulation technique.

In our simulation with the code POSINST the electrons in the cloud are represented by macroelectrons whose number is allowed to change dynamically as the build-up progresses. All macroelectrons have the same charge Q. A number $N_e = n'_{e(\gamma)} L N_b$ of photoelectrons are generated during the passage of one bunch through the dipole magnet. These N_e electrons are represented by a fixed number M_e of macroelectrons, which in most cases presented here we choose to be 1000. The macroelectron charge is given by $Q/e = N_e/M_e = n'_{e(\gamma)} L N_b/M_e$. All primary and secondary macroelectrons successively generated have the same charge.

The beam is represented by a prescribed function of space and time which in the present case is composed of a succession of proton bunches with trigaussian distribution. The bunch length is divided into $N_k - 1$ equal-length slices, corresponding to N_k kicks. This defines a simulation time step Δt. The empty space between bunches is divided into time steps of the same length Δt. The space-charge (EC self-forces) are computed by means of a 6 mm $\times$ 6 mm transverse (2D) grid. The self-field is computed and applied to the macroelectrons at every time step.

III. RESULTS

Our main results are shown in Fig. 2. For the case $t_b = 25$ ns and $N_b = 1 \times 10^{11}$ our results show that $\delta_{\max}$ must be below ~ 1.3 if the cooling capacity of the cryogenic system is not to be exceeded. For $t_b = 75$ ns the power deposition is well below the cooling capacity even for $\delta_{\max} = 2$ and $N_b = 1.6 \times 10^{11}$. The values of the power deposition in Fig. 2 are obtained from a simulation in which a single batch of 810 buckets is injected into an empty arc dipole magnet, with 72 or 24 bunches, depending on t_b. As discussed below, this single-batch calculation underestimates the power deposition.

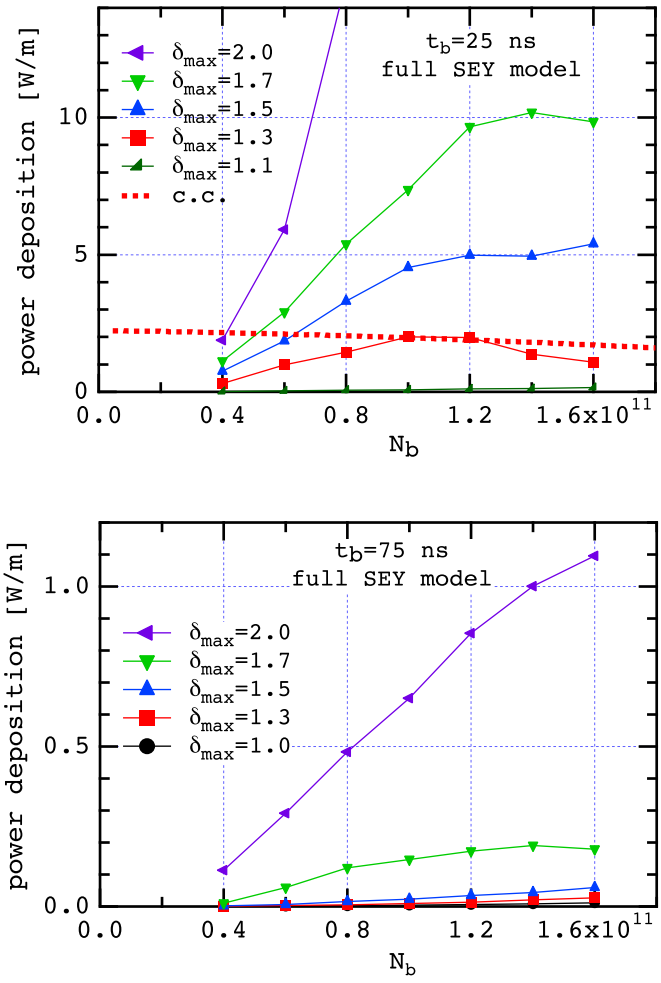

FIG. 2: Power deposition vs. bunch intensity N_b. Top: $t_b = 25$ ns. Bottom: $t_b = 75$ ns. Each curve, labeled by $\delta_{\max}$, represents a specific model for primary and secondary electron emission, corresponding to each line on Tab. II. The red dotted line is the maximum cooling capacity of the cryogenic system, taken from Ref. 1. In the top plot, for the case $\delta_{\max} = 2$, the power deposition saturates at ~ 22 W/m at $N_b \sim 1.6 \times 10^{11}$. The values of the power deposition are obtained from a single batch of 810 buckets injected into an empty arc dipole, of which either 72 or 24 are filled, depending on t_b. The nominal specification for the LHC is $N_b = 1.1 \times 10^{11}$.

TABLE I: Assumed parameters for EC simulations.

Parameter	Symbol [unit]	Value
Ring and beam parameters		
Beam energy	E [TeV]	7
Relativistic beam factor	γ_b	7460.5
Beam pipe cross section	$\cdots$	elliptical
Beam pipe semi-axes	(a, b) [cm]	(2.2,1.8)
Circumference	C [m]	26658.883
Harmonic number	h	35640
RF wavelength	$\lambda_{\rm RF}$ [m]	0.748
RF period	$T_{\rm RF}$ [ns]	2.5
Bunch spacing	t_b [ns]	25 or 75
Bunch spacing [a]	s_b [m]	7.48 or 22.44
Bunch spacing [a]	$\cdots$ [buckets]	10 or 30
Bunch train length [c]	$\cdots$ [buckets]	810
No. bunches per batch [a]	$\cdots$	72 or 24
Bunch population	N_b	$(0.4 - 1.6) \times 10^{11}$
RMS bunch length	σ_z [cm]	7.5
Longit. bunch profile	$\cdots$	gaussian
Transverse bunch profile	$\cdots$	gaussian
Transverse RMS bunch sizes	(σ_x, σ_y) [mm]	(0.3,0.3)
Simulated section	$\cdots$	arc dipole magnet
Length of simulated region	L [m]	14.2
Dipole magnet field	B [T]	7.39
Electron parameters		
Peak SEY [b]	$\delta_{\rm max}$	$1.0 - 2.0$
Photoelectron generation rate [b]	$n'_{e(\gamma)}$ [(e/p)/m]	$(0.5 - 1.2) \times 10^{-3}$
Energy at peak SEY [b]	$E_{\rm max}$ [eV]	$227.6 - 251.4$
SEY at 0 energy [b]	$\delta(0)$	$0.31 - 0.63$
Backscattered component at $E_{\rm max}$	$R_e(E_{\rm max})$	0.1
Effective photon reflectivity	R_γ	0.2
RMS height of illuminated region	σ_γ [mm]	1.4
Photoelectron angular distribution param.	α_γ	2
Photoelectron spectrum parameters	$(E_\gamma,\ \sigma_{E\gamma})$ [eV]	(5,5)
Simulation parameters		
No. kicks/bunch	N_k	21
(Full bunch length)/(RMS bunch length)	L_b/σ_z	5
Time step	Δt [s]	6.25×10^{-11}
No. primary macroelectrons/bunch passage	M_e	1000
Macroelectron charge at $N_b = 1 \times 10^{11}$	Q [e]	1.03×10^6
Space-charge grid	(h_x, h_y) [mm]	6×6

[a] First(second) value is for $t_b = 25(75)$ ns.

[b] See Table II for details.

[c] See footnote 1.

TABLE II: Assumed input parameters.

$\delta_{\max}$	$E_{\max}$ [eV]	$\delta(0)$	$\delta_{\rm nr}(0)$	$n'_{e(\gamma)}$ [(e/p)/m]
1.0	227.6	0.31	0.26	5.08×10^{-4}
1.1	230.0	0.35	0.28	5.81×10^{-4}
1.3	234.7	0.41	0.34	7.26×10^{-4}
1.5	239.5	0.36	0.39	8.71×10^{-4}
1.7	244.2	0.40	0.44	1.02×10^{-3}
2.0	251.4	0.63	0.52	1.23×10^{-3}

A. Numerical Convergence.

In order to have an idea of the numerical convergence of our calculation, we carried out two tests in which we: (a) doubled the number of primary macroelectrons per bunch passage M_e, and (b) halved the time step Δt. In case (a) the macroelectron charge Q is automatically halved while the number of macroelectrons in existence at any given time is doubled. In case (b) the number of kicks per bunch N_k is 41 instead of 21. We carried out these two tests one at a time, not in combination, and only for the case defined by $t_b = 25$ ns, $\delta_{\max} = 1.3$ and $N_b = 1 \times 10^{11}$, which we refer to as the "reference case." Other parameters for this case are listed in Tables I and II. As seen in Fig. 3 there is good agreement with the reference case. Other quantities (not shown) such as the electron energy spectrum, also shows good agreement. These results strongly suggests, but do not prove, adequate numerical convergence.

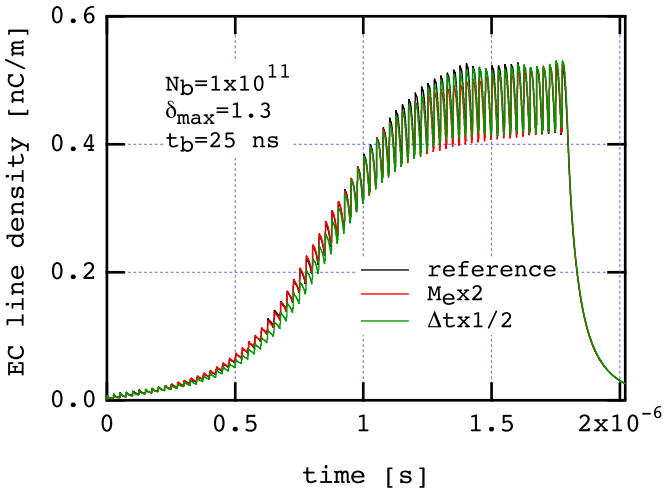

FIG. 3: Average EC line density vs. time for: reference case; doubling M_e; and halving Δt. The good agreement among the three cases indicates good numerical convergence.

B. Two Batches.

We also carried out a test case in which we simulated the EC build-up during two successive batches rather than one, again for the previously defined reference case. As seen in Fig. 4, it is clear that it takes two batches for the EC to sensibly reach steady state. Although the saturation value of the EC line density is clearly reached during the 1st batch, this saturated value is reached significantly earlier during the 2nd batch because the remnant of the EC at the end of the first gap seeds the build-up

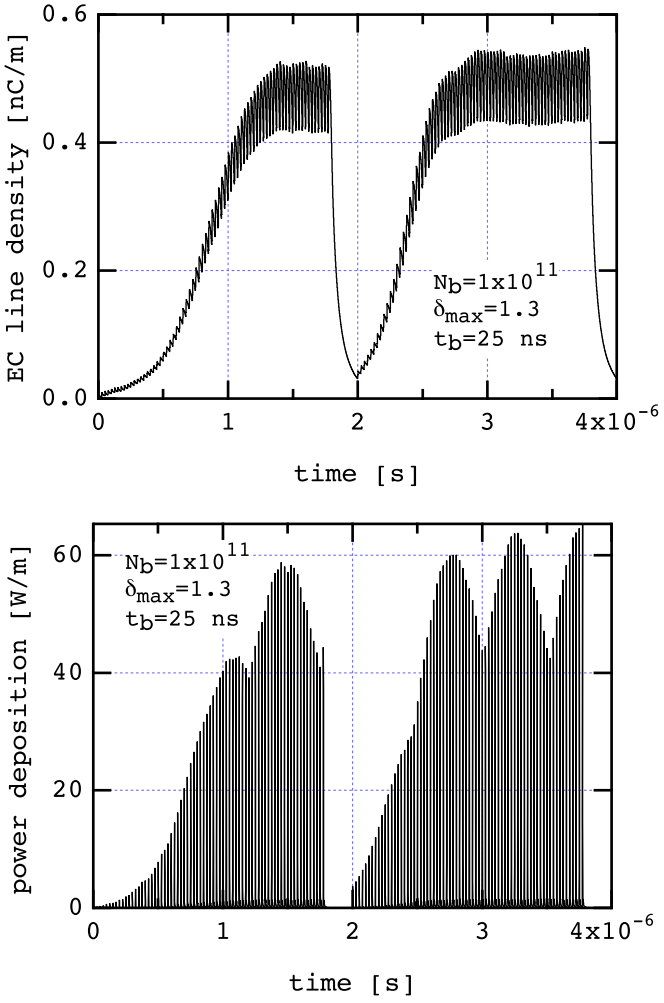

FIG. 4: Average EC line density and EC power deposition vs. time for two batches. The EC line density saturates at $\sim$ 0.5 nC/m, or $\sim$ 25% of the average beam line density, $\lambda_b = eN_b/s_b = 2.14$ nC/m. The power deposition averaged over the 1st batch is 2 W/m (this is the value shown in Fig. 2a for $\delta_{\max} = 1.3$ and $N_b = 1 \times 10^{11}$), but it is 2.8 W/m when averaged over the 2nd batch. The fact that the EC line density values at the beginning and at the end of the 2nd batch are roughly equal strongly suggests that a steady state is sensibly reached after only two batch passages. The oscillations in the power deposition with a period ~ 0.5 μs remain to be explained.

during the 2nd batch passage. As a result, the estimated power deposition during the 2nd batch is 2.8 W/m, as opposed to 2 W/m in the 1st batch.

C. Twice the Photoemission Rate.

We also carried out a test case in which the photoelectron generation rate was doubled twice the reference case, shown in Table II for $\delta_{\max} = 1.3$. As seen in Fig. 5, it is clear that although the initial rate of increase of the electron density is twice the reference case, as it should be expected, the saturated value is essentially unchanged. As a result, the estimated power deposition (not shown) increases only by $\sim 10\%$ relative to the reference case. This result implies that the power deposition is not very sensitive to details of the photoemission process such as the quantum efficiency.

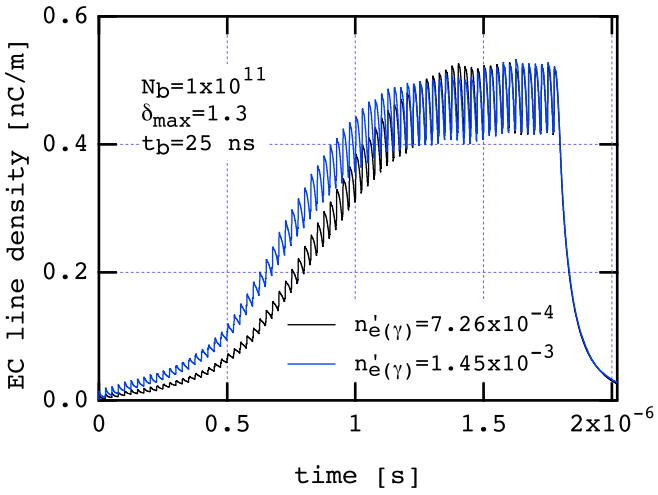

FIG. 5: Average EC line density vs. time when the photoemission rate is doubled while all other quantities are held fixed.

D. Narrower Angular Emission Distribution.

In all simulation results presented here, we assumed that the secondary emission angular distribution is uncorrelated with the emission energy, and

$$\frac{dN}{d\Omega} \propto \cos\theta \tag{3}$$

where θ is the angle of the emitted secondary electron relative to the normal to the surface at the emission point. We ran one test for the reference case in which the distribution was $\propto \cos^2\theta$ instead of $\cos\theta$, while all other parameters were kept fixed. The resultant power deposition for the 1st batch (not shown) was ~ 2.2 W/m, an increase of $\sim 10\%$ over the reference case.

IV. THE EFFECT OF REDIFFUSED ELECTRONS.

In the early simulations for the LHC arc dipoles it was noted that when the backscattered electrons were included in the simulation model, the estimate for the power deposition increased significantly compared to the case in which only the true secondary electrons were taken into account [2, 9]. The backscattered electrons[2] modify the SEY function $\delta(E_0)$ only for $E_0 \lesssim 10-20$ eV, chiefly by adding a nonzero contribution to $\delta(0)$. Given that $\delta_{\max}$ was kept fixed in those simulations, it was puzzling at first that a relatively small change in $\delta(E_0)$ would lead to a large effect in the estimate of the power deposition.

In Ref. 12 we sketched an explanation for the this large effect. The explanation focused not on the SEY function $\delta(E_0)$ but on the electron emission spectrum, which is qualitatively different for the backscattered electrons from the true secondary electrons for *most values of* E_0, not just at low energy.

In this section we provide a more detailed explanation than that provided in Ref. 12. For these purposes we contrast simulation results for both SEY models, namely with and without rediffused electrons. When we suppress the rediffused electrons we increase the elastically backscattered and true secondary components by a common factor so that $\delta_{\max}$ remains fixed. Figure 6 shows the two SEY curves for the case $\delta_{\max} = 1.3$. It is clear that they differ very little from each other in the energy range of interest which is typically 0 to a few hundred eV.

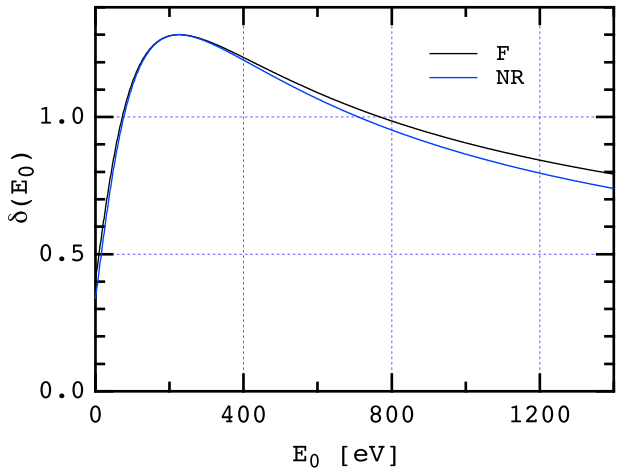

FIG. 6: SEY function $\delta(E_0)$ for $\delta_{\max} = 1.3$, for the full SEY model, and for the model in which the rediffused component is suppressed.

[2] We use the term "backscattered" to collectively describe the rediffused plus elastically backscattered electrons.

Consider first the results for the power deposition, shown in Fig. 7. It is clear that the full SEY model leads to a factor ~ 2 larger power deposition relative to the model without rediffused electrons. The results for the no-rediffused model are in good agreement with those in Ref. 1, as it should be expected, since the model used to obtain the latter results does not include rediffused electrons.

In order to explain the importance of the rediffused electrons, we now present the time dependence of several quantities. For brevity we confine ourselves to the above-mentioned reference case ($\delta_{\max} = 1.3$). Figure 8 shows the average electron-wall collision energy for a subset of four bunches in the batch. The full SEY model leads to two waves of electrons striking the walls: the 1st wave is made up of the electrons in the bulk that were kicked by the beam and struck the walls some 3 ns after the bunch passage. The 2nd wave is mostly composed of rediffused electrons that were generated when the 1st wave hit the wall. This 2nd wave is largely absent in the model with suppressed rediffused electrons. For the same time interval, Fig. 9 shows the effective SEY.[3] The 1st wave leads to substantially the same effective SEY, but the 2nd wave leads to an enhancement in the full model owing to the higher electron-wall collision energies (~ 100 eV, as seen in Fig. 8, where $\delta(E_0)$ rises above unity). The larger effective SEY, in turn, leads to roughly twice the EC density (Fig. 10) for the full model relative to the no-rediffused model, which leads to a higher power deposition (Fig. 11). The 2nd wave of electrons deposits a small amount of additional energy.

It should be remarked that, just like for the full model, the power deposition computed from the 1st batch underestimates the steady-state value by $\sim 40\%$. Indeed, for the 1st batch in the no-rediffused model in Fig. 10 we obtain 1 W/m, while for the 2nd batch we obtain 1.4 W/m. For the full model the corresponding results are 2 W/m and 2.8 W/m, respectively. As explained in the previous paragraph, most of the power is deposited by the electrons in the bulk upon being kicked by the beam (1st wave of electrons striking the walls). This suggests that the power deposition is directly proportional to the average EC density. This is indeed borne out by our results: for the no-rediffused model the average EC line density is 0.14 and 0.22 nC/m, respectively, for the 1st and 2nd batch. For the full model the corresponding results are 0.25 and 0.37 nC/m. Comparing with the corresponding values of the power deposition we arrive at the proportionality

$$\frac{\text{aver. power deposition [W/m]}}{\text{aver. EC line density [nC/m]}} \simeq 8, \qquad (4)$$

This proportionality factor of 8, valid for either batch and for either SEY model, should not be assumed to be universal; it is likely to be sensitive to N_b and possibly other parameters.

V. SUMMARY AND DISCUSSION

For the nominal LHC conditions $t_b = 25$ ns and $N_b = 1 \times 10^{11}$, our main conclusions are: (a) The cooling capacity of the cryogenic system will be exceeded by the power deposited by the EC if $\delta_{\max} \gtrsim 1.3$. (b) The EC power deposition is not very sensitive to the photelectric yield. (c) The EC power deposition is sensitive to the existence of rediffused electrons in the SEY spectrum: if we neglect the rediffused electrons, we find good agreement with CERN simulation results [1]; if we include them at a level indicated by laboratory measurements, our power deposition estimates are approximately doubled. (d) We have described in fair detail the mechanism responsible for the relatively large contribution of the rediffused electrons.

For $t_b = 75$ ns bunch spacing we find that the EC power deposition is comfortably below the cooling capacity of the cryogenic system even for $\delta_{\max} = 2$ and $N_b = 1.6 \times 10^{11}$, in qualitative agreement with Ref. 1.

The above conclusions are based on power deposition calculations for a single batch injected into an empty chamber. We have shown, however, that these single-batch results underestimate the power deposition by $\sim 40\%$ relative to the steady-state value (which is achieved after two or more batches), hence $\delta_{\max}$ may be required to be less than 1.3 for the power deposition not to exceed the cooling capacity at $N_b = 1 \times 10^{11}$. On the other hand, the actual LHC beam will have many gaps of various lengths, hence we can only conclude from our results that the actual power deposition *for any given batch* is in the range 2–2.8 W/m or, in other words, that the energy deposited is in the range 4–5.6 μJ/m per batch, the actual value depending on which specific batch one considers. An accurate calculation of the power deposition in one revolution necessitates the simulation of the full beam, taking into account all batches and gaps.

Some of the parameters in the model of electron emission we have used are correlated, as specified in Table II. The correlations between $\delta_{\max}$, $E_{\max}$ and $n'_{e(\gamma)}$ are suggested by experimental observations, and bring the input to our model closer to the assumptions used in Ref. 1. On the other hand, we have, for convenience, introduced a proportionality between $\delta(0)$ and $\delta_{\max}$ that is not used in Ref. 1, and that might not be supported by observations, as discussed further below.

We have shown in this article that the rediffused component of the secondary emission spectrum is important. It is sometimes assumed, incorrectly, that this component affects only the secondary electrons emitted at very low incident energy E_0. In fact, the backscattered component of the SEY, while maximum at low E_0, does not

[3] By "effective SEY" we mean the SEY averaged over all electron-wall collision events during a given time interval, which in this case was chosen to be 1 ns.

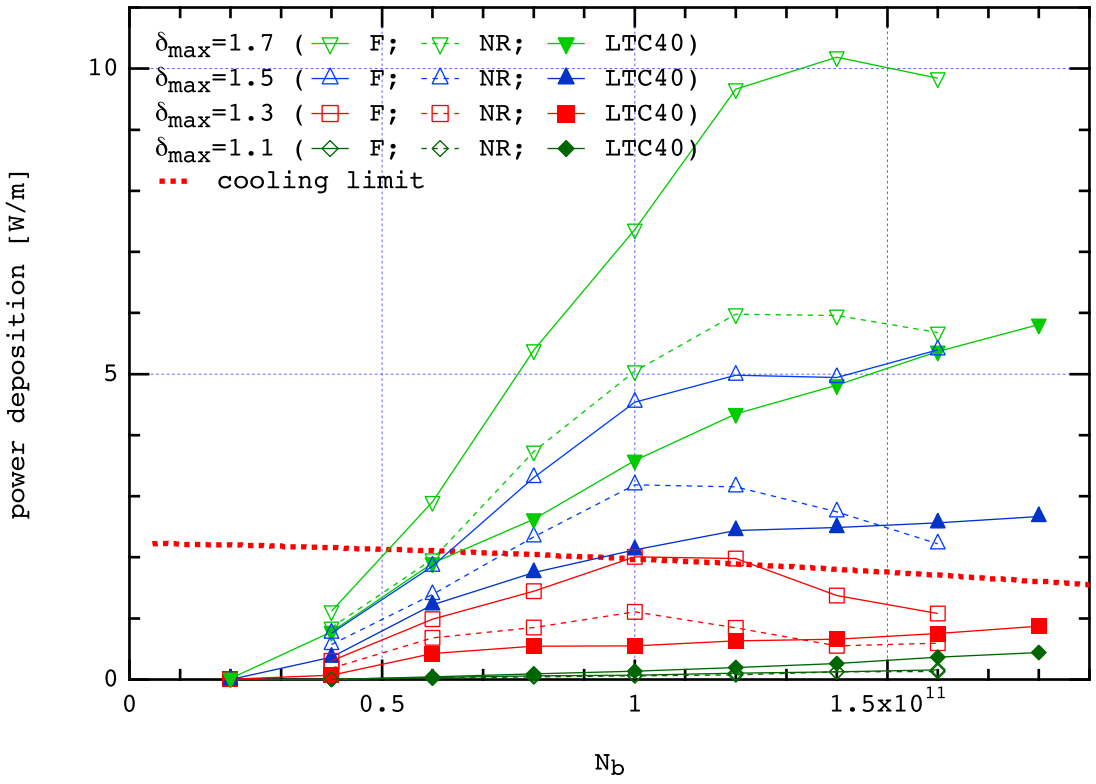

FIG. 7: Simulated power deposition. F: full SEY model. NR: no-rediffused model. LTC40: results from Ref. 1.

decrease below $\sim 0.2 - 0.3$ even in the multi-keV range [19, 20] for most materials. For the model we used here, the absolute and fractional backscattered components are shown in Fig. 1.

The ECE is a self-conditioning effect in the sense that $\delta_{\max}$ gradually decreases with normal machine operation owing to the surface conditioning from the EC bombardment, as experienced showed at the SPS [13]. It is generally expected that, as the LHC is operated, so too will $\delta_{\max}$ eventually fall below a value where the EC will no longer be an operational limitation. If we take our results as valid guidance, then it will be interesting to calculate the amount of integrated beam current required for $\delta_{\max}$ to fall below 1.3. Lab measurements at room temperature show that the bombardment required for this level of conditioning to be reached is in the range $\sim$0.1–1 C/cm^2 [14, 15]. We are not aware, however, of similar measurements at cryogenic temperatures. It is not clear, therefore, that we can apply this criterion to the case of the LHC arc dipoles.

The importance of $\delta_r(E_0)$ raises an interesting question for the conditioning process: does the backscattered component condition at the same rate that the true secondary component does? There is indirect evidence that this is not the case; in fact the evidence is consistent with the hypothesis (but does not prove it) that the backscattered component does not condition, and that only the true secondary emission component gradually decreases with electron bombardment [21, 22]. In the simulations presented in this note we have assumed that $\delta_r(E_0)$ is proportional to $\delta_{\max}$ when we varied this latter parameter. Therefore, if the above-mentioned hypothesis is correct, the actual EC power deposition might be higher, for a given $\delta_{\max}$, than the simulated estimates presented here.

Acknowledgments

We are indebted to Frank Zimmermann and Daniel Schulte for discussions on their work on the electron-cloud. We are grateful to NERSC for supercomputer support and to the DOE Office of Science Undergraduate Laboratory Internship (SULI) Program.

[1] F. Zimmermann, "Update on LHC electron-cloud simulations," LTC meeting #40, CERN, 6 April 2005, http://edms.cern.ch/lhc_proj/plsql/lhcp.page?p_number=

7700

[2] M. A. Furman, "The Electron-Cloud Effect in the Arcs of the LHC," LBNL-41482/CBP Note 247/LHC Project Report 180, 20 May 1998.

[3] G. Rumolo, F. Ruggiero, and F. Zimmermann, "Simulation of the Electron-Cloud Build Up and its Consequences on Heat Load, Beam Stability, and Diagnostics," PRST-AB **4**, 012801 (2001).

[4] Electron cloud in the LHC website, http://ab-abp-rlc.web.cern.ch/ab%2Dabp%2Drlc%2Decloud/

[5] Proc. Mini-Workshop on Electron-Cloud Simulations for Proton and Positron Beams ECLOUD'02 (CERN, Apr. 15–18, 2002), CERN Yellow Report CERN-2002-001 (F. Zimmermann and G. Rumolo, eds., 2002). http://slap.cern.ch/collective/ecloud02/

[6] Proc. 31st ICFA Advanced Beam Dynamics Workshop on Electron-Cloud Effects ECLOUD'04 (Napa, California, April 19-23, 2004), CERN Yellow Report CERN-2005-001/CARE-Conf-05-001-HHH/LBNL-56372/SNS-10400000-TR0024-R00 (M. Furman, S. Henderson and F. Zimmermann, eds., 2005); http://icfa-ecloud04.web.cern.ch/icfa-ecloud04/

[7] F. Zimmermann, E. Benedetto, F. Ruggiero, D. Schulte (CERN); M. Blaskiewicz, L. Wang (BNL); G. Bellodi (RAL); G. Rumolo (GSI); K. Ohmi, S. S. Win (KEK); M. Furman (LBNL); Y. Cai, M. T. F. Pivi (SLAC); V. K. Decyk, W. Mori (UCLA); A. F. Ghalam, T. Katsouleas (USC), "Review and Comparison of Simulation Codes Modeling Electron-Cloud Build Up and Instabilities," Proc. EPAC04 (Lucerne, 5–9 July 2004) paper THPLT017; http://accelconf.web.cern.ch/AccelConf/e04/PAPERS/THPLT017.PDF

[8] O. Gröbner, "Bunch-Induced Multipacting," Proc. PAC97, p. 3589 (Vancouver, BC, May 12–16, 1997).

[9] F. Zimmermann, "Electron-Cloud Effects in the LHC," Proc. ECLOUD'02, Ref. 5

[10] M. Furman and M. Pivi, "Microscopic Phenomenological Model for the Secondary Emission Process," talk presented by M. Furman at the ECLOUD'02 workshop, Ref. 5. This talk is not in the proceedings, but can be accessed from the talks website, http://cern.ch/conf-ecloud02/talks/furman_ECLOUD02_3_02.pdf

[11] M. A. Furman and M. Pivi, "Electron-Cloud Simulation Results for the SPS and Recent Results for the LHC," LBNL-50765, CBP Note-439, July 1st, 2002, Proc. EPAC02, Paris, June 3-7, 2002. http://accelconf.web.cern.ch/accelconf/e02/default.htm

[12] M. A. Furman, "Formation and Dissipation of the Electron Cloud," LBNL-51829; Proc. PAC03 (Portland, OR, May 12-16, 2003), paper TOPC001.

[13] J. M. Jiménez et. al., "Electron Cloud with LHC-Type Beams in the SPS: A Review of Three Years of Measurements," LHC Project Report 632, 8 April 2003.

[14] R. E. Kirby and F. K. King, "Secondary Electron Emission Yields From PEP-II Accelerator Materials," SLAC Report No. SLAC-PUB-8212, 2000; NIMPR **A469**, 1-12 (2001).

[15] V. Baglin, I. Collins, B. Henrist, N. Hilleret, G. Vorlaufer, "A Summary of Main Experimental Results Concerning the Secondary Electron Emission of Copper," LHC Project Report 472, 2 August 2001.

[16] M. A. Furman and G. R. Lambertson, "The Electron-Cloud Instability in the Arcs of the PEP-II Positron Ring," LBNL-41123/CBP Note-246, PEP-II AP Note AP 97.27, November 25, 1997; Proc. Intl. Workshop on Multibunch Instabilities in Future Electron and Positron Accelerators (MBI-97), KEK, Tsukuba, Japan, 15–18 July 1997, KEK Proceedings **97-17**, Dec. 1997 (Y. H. Chin, ed.), p. 170.

[17] M. A. Furman and M. T. F. Pivi, "Probabilistic Model for the Simulation of Secondary Electron Emission," LBNL-49771, CBP Note-415, November 6, 2002, http://prst-ab.aps.org/pdf/PRSTAB/v5/i12/e124404.

[18] M. A. Furman and M. T. F. Pivi, "Simulation of Secondary Electron Emission Based on a Phenomenological Probabilistic Model," LBNL-52807/SLAC-PUB-9912, June 2, 2003.

[19] D. C. Joy, "A Database on Electron-Solid Interactions," Scanning **17**, 270-275 (1995). The database can be downloaded from http://pciserver.bio.utk.edu/metrology/htm/home.shtml

[20] Backscattered electron data and simulation tools can be obtained from the website MC-SET: Monte Carlo Simulation of Electron Trajectories, http://www.napchan.com/

[21] R. Cimino, I. R. Collins, M. A. Furman, M. Pivi, F. Ruggiero, G. Rumolo, and F. Zimmermann, "Can Low Energy Electrons Affect High Energy Physics Accelerators?," CERN-AB-2004-012 (ABP), LBNL-54594, SLAC-PUB-10350, February 9, 2004; Phys. Rev. Lett. **93**, 014801 (2004).

[22] R. Macek, M. Borden, A. Browman, D. Fitzgerald, R. McCrady, T. Spickermann, T. Zaugg, "Status of the Experimental Studies of the Electron Cloud at the Los Alamos Proton Storage Ring," Proc. PAC03 (Portland, OR, May 12-16, 2003), paper RPPB035.

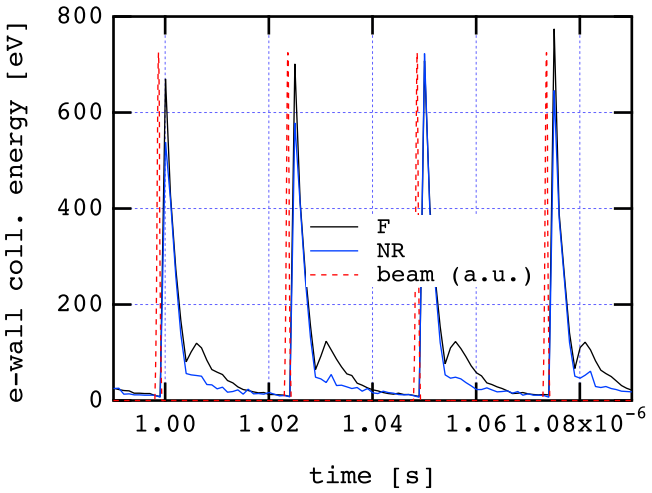

FIG. 8: Average electron-wall collision energy per electron vs. time for bunches #41–44 in the 1st batch for the reference case. F: full model. NR: no-rediffused model. Red dotted line: beam signal (arbitrary units). Some $\sim$ 3 ns after the bunch passage the electrons kicked by the beam strike the walls. Some $\sim$ 5 ns later, a second wave of electrons hits the walls, most of which are rediffused electrons generated when the 1st wave struck the wall. The 2nd wave is substantially absent in the no-rediffused model.

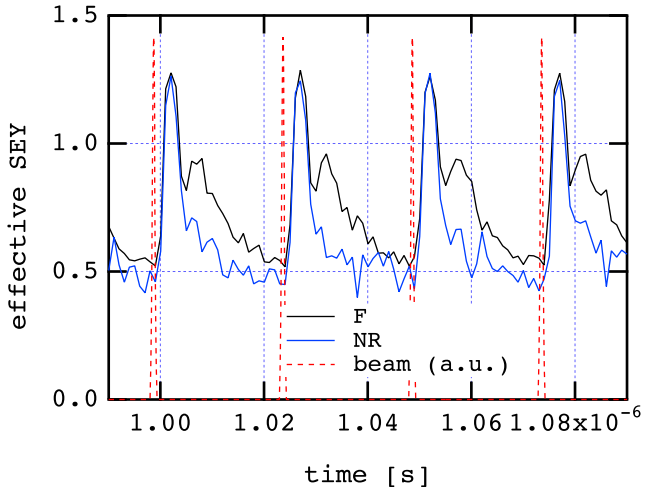

FIG. 9: Effective secondary emission yield vs. time for the same bunches shown in Fig. 8. The 2nd wave of electrons leads to a higher effective SEY in the full model compared with the no-rediffused model, owing to their higher average wall collision energy.

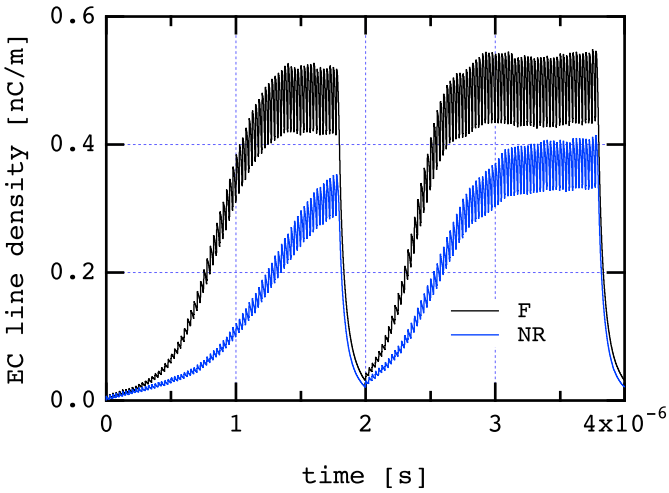

FIG. 10: Average EC line density vs. time. The higher effective SEY in the full model leads to $\sim$twice the EC density in the 1st batch, as compared with the no-rediffused model.

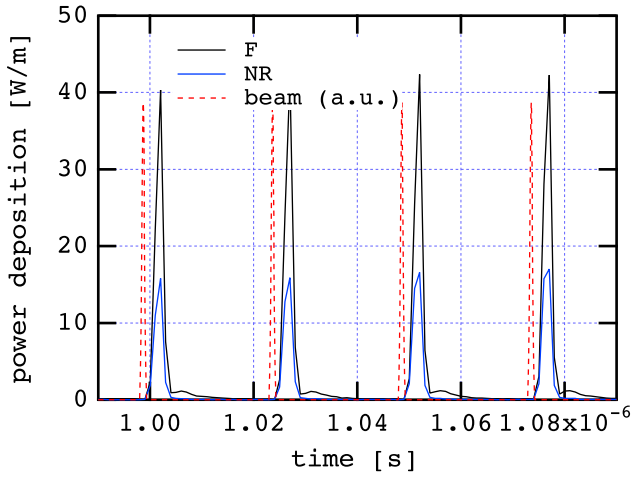

FIG. 11: Average power deposition vs. time. The higher EC density for the full model leads to $\sim$twice the power deposition in the 1st batch relative to the no-rediffused case. Most of the power is deposited by the 1st wave of electrons, but an additional 5–10% is deposited by the 2nd wave of electrons in the full model.